IET Radar, Sonar & Navigation

Research Article

Estimation of range-dependent sound-speed profile with dictionary learning method

ISSN 1751-8784
Received on 24th March 2019
Revised 8th November 2019
Accepted on 15th November 2019
doi: 10.1049/iet-rsn.2019.0107
www.ietdl.org

Yu-Hsin Kuo[1], Jean-Fu Kiang[1] ✉
[1]*Graduate Institute of Communication Engineering, National Taiwan University, Taipei 106, Taiwan*
✉ *E-mail: jfkiang@ntu.edu.tw*

Abstract: A range-dependent dictionary learning method is proposed to retrieve the sound-speed profile (SSP) in a water body, with the whole computational domain decomposed into multiple range-independent subdomains. A dictionary is constructed by using the World Ocean Atlas depth profiles of temperature and salinity. The simulation results verify the efficacy of the dictionary in retrieving the range-independent SSP profile in each subdomain.

1 Introduction

The behaviour of acoustic waves in a water body is determined by its sound-speed profile (SSP). Applications like submarine warfare demand source localisation, which relies on accurate prior information of SSP [1, 2]. The channel capacity for underwater acoustic communications is also dependent on prior SSP information [3]. The SSP near sea surface is affected by wind speed and rainfall rate above sea surface, which can in turn be estimated from the SSP [4].

In general, the SSP is closely related to the depth profiles of temperature and conductivity in the water body [5]. A conductivity-temperature-depth (CTD) device was usually deployed to measure the temperature and electric conductivity at different depths, from which to retrieve the SSP. However, it is impractical to monitor the SSP with such devices in a vast area over long time period [5, 6]. Alternative methods include an acoustic inversion approach to monitor rapidly changing SSP [5], travel-time data collected with an ocean acoustic tomography (OAT) technique [7] or matched field inversion [8–10].

An empirical orthogonal function (EOF) analysis models an SSP in terms of a few leading-order EOFs [11, 12], of which the coefficients are obtained by applying ensemble Kalman filter, no-trace Kalman filter or particle filter [13]. However, the requirement of orthogonality limits its efficacy of regularisation and resolution [11, 12]. Schmidt *et al.* proposed an acoustically focused oceanographic sampling method to improve the resolution under rapidly changing environment [14, 5]. A conventional OAT method was applied first to get low-resolution results, followed by dispatching a moving sensor like autonomous underwater vehicle (AUV) to high-uncertainty areas to collect small-scale high-resolution data [5]. However, significant Doppler shift from high-frequency sources may compromise the data, even at slow moving speed of sensor [9].

In [11, 12], a dictionary learning method equipped with a K-SVD algorithm [15] was used to retrieve SSP. Since the dictionary learning method is not restrained by orthogonality, it is more flexible to model wider variation of SSP [12]. It was reported that the SSP retrieved with the dictionary learning method was more accurate than that with the EOF analysis [11].

In most literature, the SSP was approximated to depend only on depth but not range, which was not accurate enough for some long-range applications where SSP at one end is significantly different from that at the other end [16]. In [17], a range-independent EOF was extended to a range-dependent version to increase its prediction accuracy, with prior information from the Navy Coastal Ocean Model. The computational domain of 15 km by range and 110 m by depth was segmented into seven subdomains. With one transmitter and 48 receivers at 2 m spacing, the maximum root-mean-square error of retrieved SSP was about 0.9 m/s.

In this work, we propose a range-dependent OAT method, in which candidate SSPs are represented by atoms in a well-prepared dictionary [10, 18]. The whole computational domain is segmented into multiple subdomains, each characterised by a range-independent SSP. A ray-tracing method [19] is applied to compute the ray path and time delay from one specific transmitter to one specific receiver. The time-delay perturbation along a given ray is contributed by different constituents of the ray path through different subdomains. The time-delay perturbation in each subdomain is written as a product of the environment matrix and the SSP difference in that subdomain. The environment matrices in all the subdomains are combined into one environment matrix, and then the optimisation method is applied to retrieve the SSP in the whole computational domain.

The rest of this paper is organised as follows. The algorithm for retrieving range-independent SSP with dictionary learning method is presented in Section 2, the range-dependent dictionary learning method is presented in Section 3, the method to construct a dictionary out of the World Ocean Atlas (WOA) depth profiles of temperature and salinity is presented in Section 4, the simulation results are discussed in Section 5, and some conclusions are drawn in Section 6.

2 Retrieval of range-independent SSP

Fig. 1 shows the schematic of ray paths from one transmitter, across multiple subdomains, to M_r receivers. The acoustic wave propagates at velocity $\hat{r}c$ with respect to the water body [7], where $\hat{r}$ is the ray propagation direction. If the water flows at velocity $\bar{v}$ with respect to the ocean floor, the velocity of the wave relative to the ocean floor will be $\bar{c}_m = \hat{r}c + \bar{v}$, and the acoustic velocity along the ray path will be

$$\hat{r} \cdot \bar{c}_m = c + \hat{r} \cdot \bar{v} \tag{1}$$

In a steady water-body, the SSP can be represented as

$$c(r,z) = c_0(r,z) + \delta c(r,z) \tag{2}$$

where $c_0(r,z)$ is the reference acoustic-velocity and $\delta c(r,z)$ is its perturbation.

The travel time along a ray path is more sensitive to medium perturbation than to the ray-path perturbation [18], hence the latter is neglected. We will retrieve the SSP perturbation from the travel-time perturbation. From (1) and (2), the travel time τ along a ray path between a given transmitter and a given receiver is

$$\tau = \int \frac{ds}{c} = \int \frac{1}{c_0 + \delta c + \hat{r} \cdot \bar{v}} ds \simeq \int \left(\frac{1}{c_0} - \frac{\delta c}{c_0^2} - \frac{\hat{r} \cdot \bar{v}}{c_0^2} \right) ds = \tau_0 + \delta\tau + \delta\tau_{\rm oc} \tag{3}$$

where τ_0 is the travel time in the reference SSP, $\delta\tau$ and $\delta\tau_{\rm oc}$ are the travel-time perturbations caused by SSP perturbation and water flow, respectively. Typically, $\hat{r} \cdot \bar{v} \ll c$, thus $\delta\tau_{\rm oc}$ in (3) can be neglected [10], hence $\delta\tau$ is approximated as

$$\delta\tau = \tau - \tau_0 = \int \frac{ds}{c} - \int \frac{ds}{c_0} \simeq - \int \frac{\delta c}{c_0^2} ds$$

The time-delay perturbation along the nth ray path to the mth receiver, $P_{\rm mn}$, is

$$\delta\tau_{\rm mn} = \tau_{\rm mn} - \tau_0 \simeq - \int_{P_{\rm mn}} \frac{\delta c}{c_0^2} ds \simeq - \sum_{p=1}^{N_s} \Delta s_p \zeta_{pq} \frac{\delta c}{c_0^2} \bigg|_{z = z_q} = \sum_{q=1}^{N_\ell} E_{\rm mnq} \frac{\delta c}{c_0^2} \bigg|_{z = z_q} \tag{4}$$

where ray path $P_{\rm mn}$ is decomposed into N_s segments, N_ℓ is the number of horizontal layers, with a constant sound speed in each layer, $\zeta_{\rm pq} = 1$ (or 0) if the pth segment of the ray path (with length Δs_p) falls within (or without) the depth interval centred at z_q. Equation (4) can be put in a matrix form as

$$\bar{y} = \bar{\bar{E}} \cdot \bar{x} + \bar{n} \tag{5}$$

with

$$\bar{y} = \left[\delta\bar{\tau}_1^{\rm t}, \delta\bar{\tau}_2^{\rm t}, \cdots, \delta\bar{\tau}_m^{\rm t}, \cdots, \delta\bar{\tau}_{M_r}^{\rm t}\right]^{\rm t}$$

where t stands for transpose, $\bar{n}$ contains the noise at receivers, $\delta\bar{\tau}_m$ contains the time-delay perturbations along all possible ray paths reaching the mth receiver. Explicitly

$$\delta\bar{\tau}_m = \left[\delta\tau_{m1}, \delta\tau_{m2}, \ldots, \delta\tau_{mQ_m}\right]^{\rm t}$$

where $\delta\tau_{\rm mn}$ is the time-delay perturbation along $P_{\rm mn}$, and Q_m is the number of rays reaching receiver m. The total number of time-delay perturbations in $\bar{y}$ is $Q = Q_1 + Q_2 + \cdots + Q_{M_r}$. In (5), $\bar{x}$ contains the SSP perturbations at all depth intervals, namely

$$\bar{x} = \left[\delta c_1/c_0^2, \delta c_2/c_0^2, \ldots, \delta c_{N_\ell}/c_0^2\right]^{\rm t}$$

The rqth element of $\bar{\bar{E}}_{Q \times N_\ell}$ is the length of segment along the rth ray path that passes through the qth depth interval. Equation (5) can be solved by minimising a cost function

$$J_1 = \| \bar{y} - \bar{\bar{E}} \cdot \bar{x} \|_2^2 \tag{6}$$

under L_2-norm.

Prior information can reduce the effects of noise in retrieving $\bar{x}$ [10]. We first compile a dictionary $\bar{\bar{D}}_{N_\ell \times N_a}$ with N_a atoms from prior information of SSP. The solution $\bar{x}$ is conveniently represented as a superposition of atoms in $\bar{\bar{D}}$. Since $\bar{\bar{D}}$ is usually overcomplete [10], $\bar{x}$ is better represented as a sparse linear combination of atoms in $\bar{\bar{D}}$, leading to a constrained cost function of

$$J_2 = \mu_1 \| \bar{y} - \bar{\bar{E}} \cdot \bar{x} \|_2^2 + \| \bar{x} - \bar{\bar{D}} \cdot \bar{\boldsymbol{\alpha}} \|_2^2 \quad \text{such that } \| \bar{\boldsymbol{\alpha}} \|_0 \le S_p \tag{7}$$

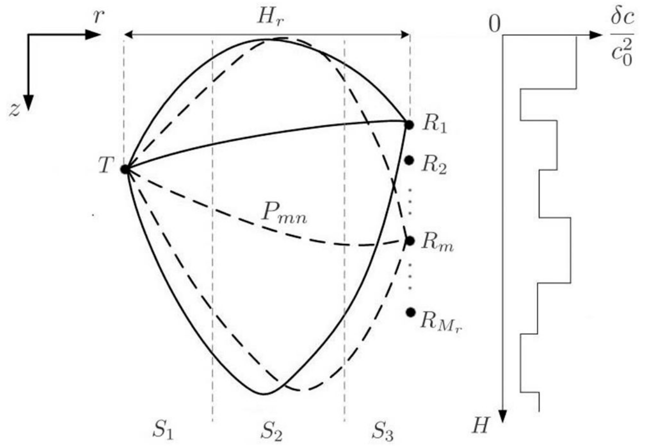

Fig. 1 *Schematic of multiple ray paths across multiple subdomains, with SSP perturbation on the right column*

where μ_1 is used to tune the relative importance of time-delay perturbation, $\bar{\boldsymbol{\alpha}}$ is an N_a-vector containing the weighting coefficients of atoms in $\bar{\bar{D}}$, S_p is a sparsity index to restrict the number of non-zero elements in $\bar{\alpha}$, specified in L_0-norm. Due to the non-convex property of L_0-norm, J_2 in (7) cannot be directly minimised [10]. A convex problem is formed by replacing the L_0-norm with L_1-norm [20], thus the cost function in (7) is modified as

$$J_3 = \mu_1 \| \bar{y} - \bar{\bar{E}} \cdot \bar{x} \|_2^2 + \| \bar{x} - \bar{\bar{D}} \cdot \bar{\boldsymbol{\alpha}} \|_2^2 + \mu_2 \| \bar{\boldsymbol{\alpha}} \|_1 \tag{8}$$

where μ_2 is used to control the sparsity of $\bar{\alpha}$.

The cost function in (8) is minimised in two steps [10]. In the first step, $\bar{\alpha}$ is computed by minimising

$$J_{3a} = \| \bar{x} - \bar{\bar{D}} \cdot \bar{\boldsymbol{\alpha}} \|_2^2 + \mu_2 \| \bar{\boldsymbol{\alpha}} \|_1 \tag{9}$$

with an orthogonal matching pursuit method, using the latest version of $\bar{x}$. In the second step, $\bar{x}$ is updated, with $\bar{\boldsymbol{\alpha}}$ from the first step, by minimising

$$J_{3b} = \mu_1 \| \bar{y} - \bar{\bar{E}} \cdot \bar{x} \|_2^2 + \| \bar{x} - \bar{\bar{D}} \cdot \bar{\boldsymbol{\alpha}} \|_2^2$$

which can be transformed to a least-square problem as

$$J_{3c} = \left\| \left[\bar{\bar{\boldsymbol{I}}} \cdot \bar{x}, \mu_3 \bar{\bar{E}} \cdot \bar{x}\right] - \left[\bar{\bar{D}} \cdot \bar{\boldsymbol{\alpha}}, \mu_3 \bar{y}\right] \right\|_2^2 = \left\| \left[\left|\bar{\bar{\boldsymbol{I}}}, \mu_3 \bar{\bar{E}}\right|\right] \cdot \bar{x} - \left[\bar{\bar{D}} \cdot \bar{\boldsymbol{\alpha}}, \mu_3 \bar{y}\right] \right\|_2^2 \tag{10}$$

where $\left[\left|\bar{\bar{\boldsymbol{A}}}, \bar{\bar{\boldsymbol{B}}}\right|\right]$ means stacking matrices $\bar{\bar{\boldsymbol{A}}}$ and $\bar{\bar{\boldsymbol{B}}}$ vertically, $\bar{\bar{\boldsymbol{I}}}$ is an $N_\ell \times N_\ell$ identity matrix, and $\mu_1 = \mu_3^2$. Equation (10) can be solved by using a pseudo-inverse technique.

3 Retrieval of range-dependent SSP

A range-dependent SSP in the whole computational domain is approximated as a cascade of range-independent SSPs, with each covering a subdomain. Fig. 1 shows an example domain segmented into three subdomains, S_1, S_2 and S_3. A ray path across the border between two adjacent subdomains is perceived as an acoustic wave being received at the border of one subdomain and then relayed to the adjacent subdomain. The total time-delay along a ray path across the whole domain is the sum of time delays across all the constituent subdomains. Similar to (5), the time-delay perturbations can be represented as

$$\bar{y} = \bar{\bar{E}}_1 \cdot \bar{x}_1 + \bar{\bar{E}}_2 \cdot \bar{x}_2 + \cdots + \bar{\bar{E}}_{M_s} \cdot \bar{x}_{M_s} + \bar{n} \tag{11}$$

where M_s is the number of subdomains, $\bar{\bar{E}}_s$ and $\bar{x}_s$ are the counterparts of $\bar{\bar{E}}$ and $\bar{x}$, respectively, in (5), in the sth subdomain. Equation (11) can be rearranged as

$$\bar{y} = \bar{\bar{E}}_c \cdot \bar{x}_c + \bar{n} \tag{12}$$

where $(\bar{\bar{E}}_c)_{Q \times N_\ell M_s}$ and $(\bar{x}_c)_{N_\ell M_s}$ are the concatenation of $(\bar{\bar{E}}_m)_{Q \times N_\ell}$ and $(\bar{x}_m)_{N_\ell}$, respectively, with $1 \le m \le M_s$.

Similar to (8), the cost function for the range-dependent problem is defined as

$$\begin{aligned} J_4 &= \mu_1 \| \bar{y} - \bar{\bar{E}}_c \cdot \bar{x}_c \|_2^2 \\ &+ \sum_{s=1}^{M_s} \left\{ \| \bar{x}_s - \bar{\bar{D}}_s \cdot \bar{\alpha}_s \|_2^2 + \mu_2 \| \bar{\alpha}_s \|_1 \right\} \end{aligned} \tag{13}$$

where $(\bar{\bar{D}}_s)_{N_\ell \times N_a}$ is the dictionary in subdomain s, and $(\bar{\alpha}_s)_{N_a}$ contains the coefficients of atoms in $\bar{\bar{D}}_s$ to represent $\bar{x}_s$. To solve (13) for $\bar{x}_c$, we first compute $\bar{\alpha}_s$ in subdomain s by minimising

$$J_{4a} = \| \bar{x}_s - \bar{\bar{D}}_s \cdot \bar{\alpha}_s \|_2^2 + \mu_2 \| \bar{\alpha}_s \|_1$$

where $\bar{x}_s$ is retrieved from the latest version of $\bar{x}_c$. Next, update $\bar{x}_c$, with the latest version of $\bar{\alpha}_s$'s, by minimising

$$J_{4b} = \mu_1 \| \bar{y} - \bar{\bar{E}}_c \cdot \bar{x}_c \|_2^2 + \sum_{s=1}^{M_s} \| \bar{x}_s - \bar{\bar{D}}_s \cdot \bar{\alpha}_s \|_2^2$$

which is rearranged to a least-square problem as

$$J_{4c} = \left\| \left[\left[\bar{\bar{I}}, \mu_3 \bar{\bar{E}}_c \right] \right] \cdot \bar{x}_c - \left[\bar{d}_\alpha, \mu_3 \bar{y} \right] \right\|_2^2 \tag{14}$$

where

$$\bar{d}_\alpha = \left[\bar{\bar{D}}_1 \cdot \bar{\alpha}_1, \bar{\bar{D}}_2 \cdot \bar{\alpha}_2, \ldots, \bar{\bar{D}}_{M_s} \cdot \bar{\alpha}_{M_s} \right]$$

These two steps are iterated until $\bar{x}_c$ converges.

4 Construction of dictionary with depth profiles from WOA18

The Del Grosso equation prescribes the sound speed at depth z (m) below water surface as a function of temperature T (°C) and salinity S (‰) as

$$\begin{aligned} c &= 1449.2 + 4.6T - 0.055T^2 + 0.00029T^3 \\ &+ (1.34 - 0.01T)(S - 35) + 0.016z \end{aligned} \tag{15}$$

The predictions with reformulated Del Grosso equation and UNESCO equation [21, 22] are different from that with (15) by <0.2 m/s, by using the WOA depth profile of T and S.

In WOA18, monthly data of mean (μ) and standard deviation (σ) of salinity and temperature are provided, with the finest resolution of quarter-degree in latitude and longitude. Note that the data are insensitive to longitude. In this work, a dictionary is constructed by using the WOA18 data issued in 2018 to generate SSP atoms [23, 24]. In a specific region of interest, the dictionary is compiled by including the WOA18 data within $\pm 1°$ in latitude and all available longitudes. To deal with temporal variation, the WOA18 data within ± 1 months are also included. At each geographical site and in each month thus included, the (T, S) profiles of μ, $\mu \pm 0.5\sigma$, $\mu \pm \sigma$, $\mu \pm 1.5\sigma$ and $\mu \pm 2\sigma$, respectively, are substituted into (15) to generate candidate SSP profiles, which will be compressed into fewer number of atoms, to be described in the next section.

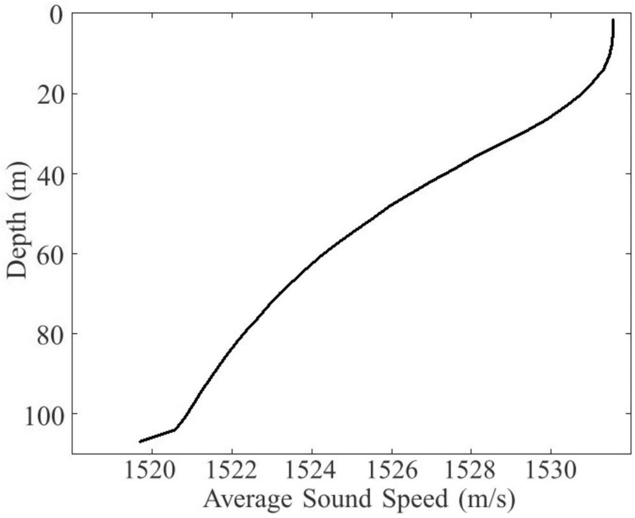

Fig. 2 *Reference SSP, $c_0(z)$, at (29.7°N, 126.8°E), May–July 2001*

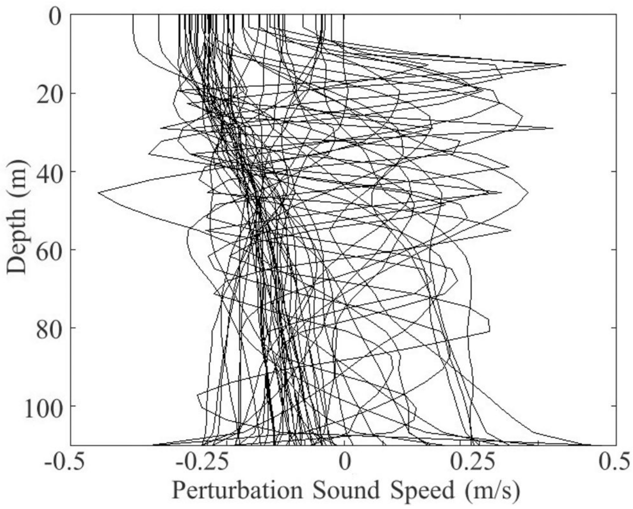

Fig. 3 *Dictionary of 53 atoms, each representing a perturbation SSP, $\delta c(z)$*

5 Simulations and discussions

Consider the Asian Seas International Acoustics Experiment (ASIAEX), which was carried out with CTD between 28 May and 9 June 2001 [25]. Fig. 2 shows the reference SSP which is derived by taking the depth-wise average of those 2000 strong candidate SSPs computed in the last section. In [10], a K-means singular value decomposition (K-SVD) method based on k-means was applied to the measurement data to construct a dictionary of 53 atoms. Fig. 3 shows the 53 atoms obtained by applying the same (K-SVD) method to the 2000 strong candidate SSPs.

5.1 Range-independent case

We choose the same range of $H_r = 2\,\text{km}$ and depth of $H = 110\,\text{m}$ as in [10]. A transmitter is placed at $r = 0$ and $z = 20\,\text{m}$, six receivers are placed at $r = 2\,\text{km}$ and $z = 20(n-1)\text{m}$, with $1 \le n \le 6$. The whole depth is segmented into $N = 35$ uniform intervals of $\Delta z = 110/35\,\text{m}$.

Fig. 4 shows a testing SSP sampled from [10] and the retrieved SSP with the proposed method. Fig. 5 shows the absolute difference between the testing SSP and the retrieved SSP, with the maximum value about 0.75 m/s, the same as in [10].

The value of μ_3 is chosen to make $\| \bar{y} \|$ comparable to $\| \bar{\bar{D}} \cdot \bar{\alpha} \|$, as in (10). In this case, $\| \bar{y} \|$ is about three orders of magnitude smaller than $\| \bar{\bar{D}} \cdot \bar{\alpha} \|$, leading to $\mu_3 = 10^3$. The value of μ_3 is tuned up if prior information in the dictionary is suspicious. On the other hand, μ_3 is tuned down if the dictionary contains credible information.

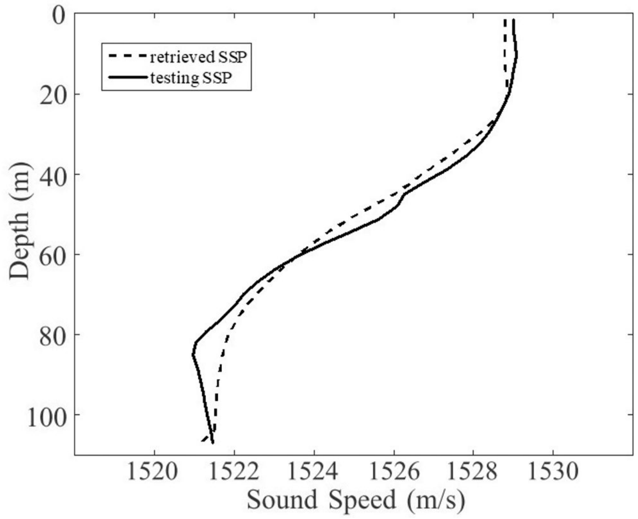

Fig. 4 *Testing SSP (---------) and its retrieval (– – –)*

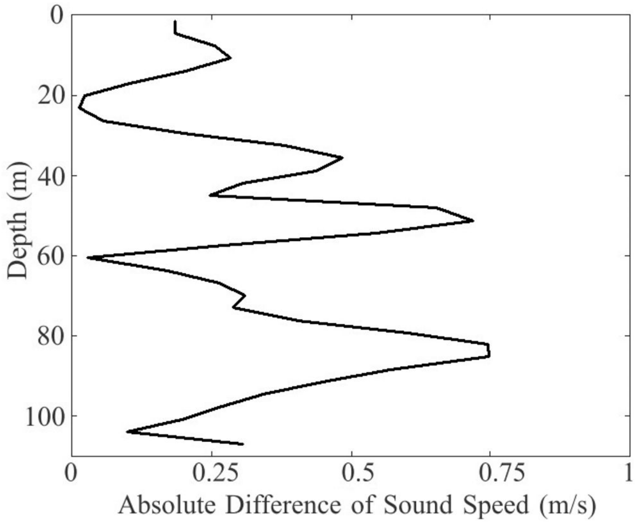

Fig. 5 *Absolute difference between testing SSP and retrieved SSP in Fig. 4*

Several testing SSPs from other references have also been compared with the retrieved SSP using the proposed method. The absolute differences are on the same order as in Fig. 5. It indicates that a dictionary constructed by applying the Del Grosso equation to the WOA18 depth profiles can retrieve credible SSP from received signals over multiple ray paths.

5.2 Range-dependent case

Consider another computational domain with a wider range of $H_r = 100\,\text{km}$ and the same depth of $H = 110\,\text{m}$. A transmitter is placed at $r = 0$ and $z = 20\,\text{m}$, and six receivers are placed at $r = 100\,\text{km}$ and $z = 20(n-1)\text{m}$, with $1 \le n \le 6$. The whole computational domain is segmented into four subdomains (S_1, S_2, S_3 and S_4), each covering a range of 25 km. The scenario is arbitrarily placed at 24°N latitude, 122 – 123°E longitude.

In the forward problem of simulating multiple ray paths and time-delay perturbation $\delta\tau_{\text{mn}}$, five SSPs are first derived from the WOA18 data at the junctions of adjacent subdomains, as well as at $r = 0$ and $r = 100\,\text{km}$. The SSP within each subdomain is linearly interpolated from the SSPs at the two ends of that subdomain. In the inverse problem, the SSPs at the middle of each subdomain will be retrieved.

Fig. 6 shows the testing SSP and its retrieved counterpart in each subdomain, with or without the dictionary. Here, without dictionary means solving (12) directly by using the pseudo-inverse method. It is observed that the retrieved SSP with dictionary has weaker ripples versus depth than that without dictionary. Fig. 7

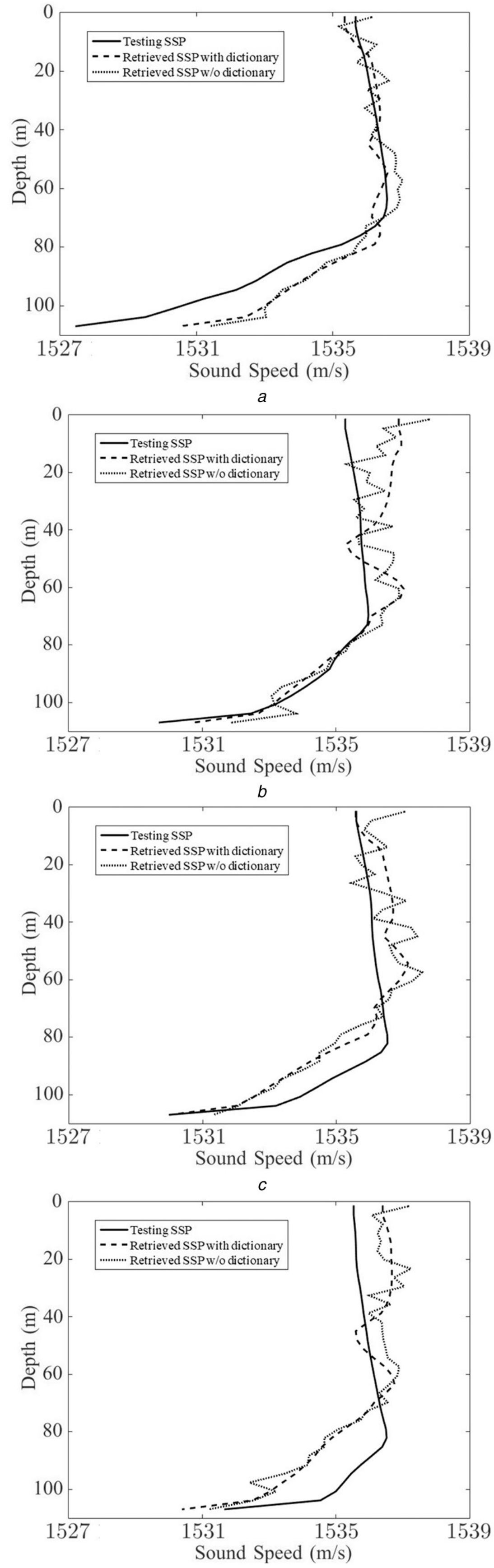

Fig. 6 *Testing SSP (---------), retrieved SSP with dictionary of 53 atoms (– – –) and retrieved SSP without dictionary (⋯) in subdomain*

(a) S_1,

(b) S_2,

(c) S_3,

(d) S_4

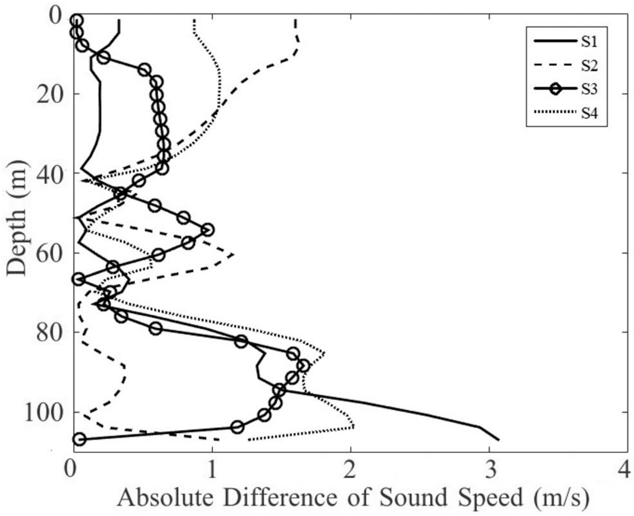

Fig. 7 *Absolute difference between testing SSP and retrieved SSP with dictionary of 53 atoms, ---------: S_1, — — —: S_2, ---∘---: S_3, ⋯: S_4*

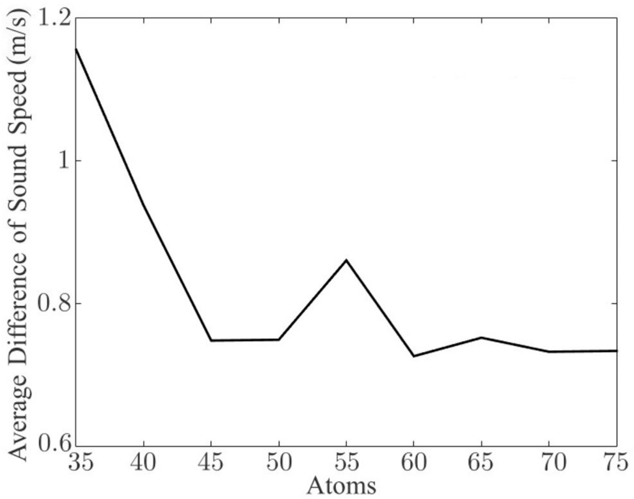

Fig. 8 *Average difference of SSP versus number of atoms in the dictionary*

shows the absolute difference between the testing SSP and the retrieved SSP with dictionary of 53 atoms.

Fig. 8 shows the average difference of sound speed over four subdomains, with 35 sample points at different depths in each subdomain. The average difference is barely reduced when more than 60 atoms are chosen.

Fig. 9 shows the testing SSP and the retrieved SSP with a dictionary of 70 atoms, and Fig. 10 shows the absolute difference between them. It is observed that the absolute difference of SSP is smaller than its counterpart in Fig. 7 at depths <70 m, but becomes larger at depths >70 m. One possible reason is that the slope of SSP changes dramatically around 70 m in subdomains S_1 and S_2, as well as around 80 and 100 m in subdomains S_3 and S_4.

6 Conclusion

A dictionary learning method has been proposed to retrieve the SSP from the received signals at multiple depths, where a dictionary is compressed from sample SSPs derived by applying the Del Grosso equation to the depth profiles of WOA18 within the geographical and temporal regions of interest. Simulations show that the range-independent SSP thus obtained is credible, as compared to the literature. A range-dependent dictionary learning method has also been proposed. With proper number of atoms in the dictionary, the absolute difference between the testing SSP and the retrieved SSP can be compatible to that in range-independent case, as long as the SSP slope does not change dramatically at certain depths.

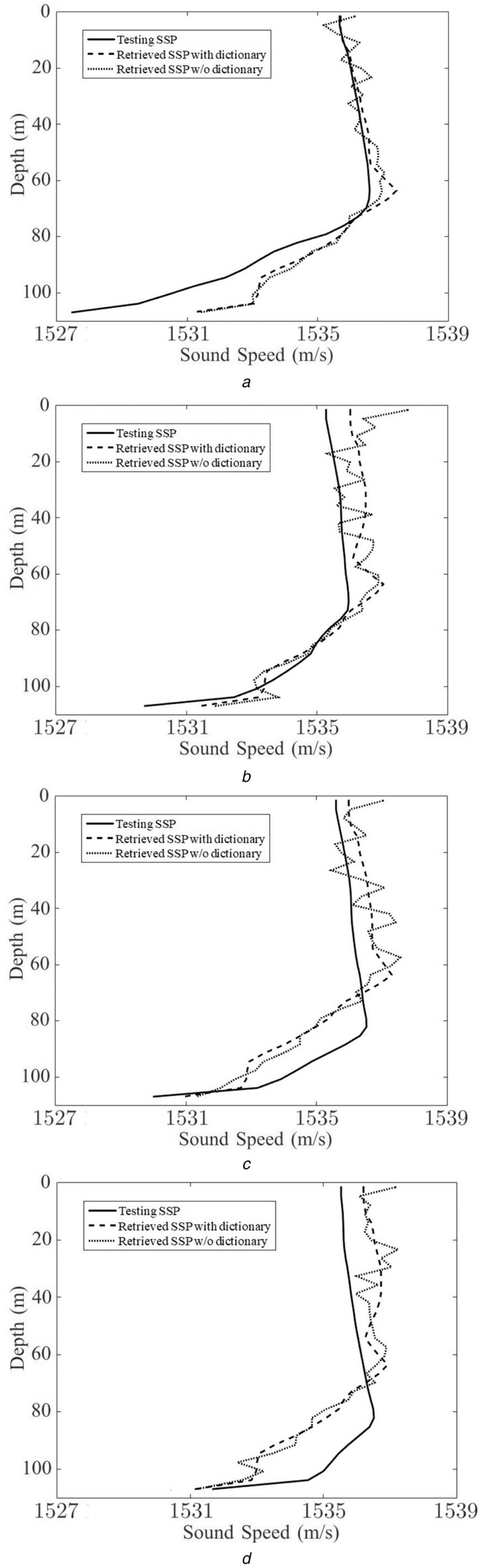

Fig. 9 *Testing SSP (---------), retrieved SSP with dictionary of 70 atoms; (— — —) and retrieved SSP without dictionary (⋯) in subdomain*
(a) *S_1,*
(b) *S_2,*
(c) *S_3,*
(d) *S_4*

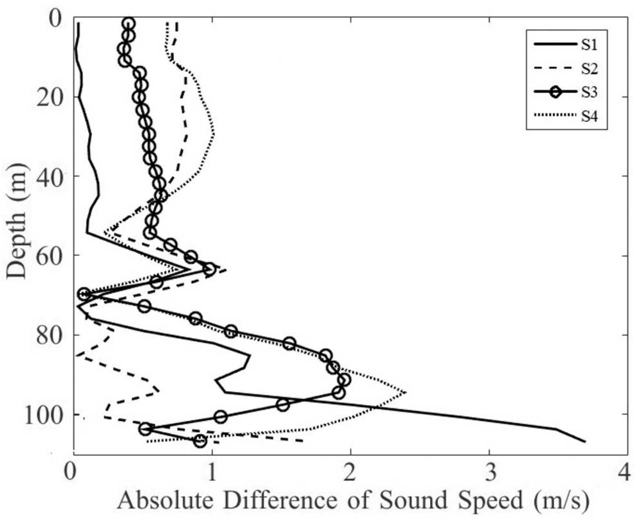

Fig. 10 *Absolute difference between testing SSP and retrieved SSP with dictionary of 70 atoms, ---------: S_1, — — —: S_2, ---∘---: S_3, ⋯: S_4*

7 References

[1] Li, C. X., Guo, M. F., Pan, X.: 'Effect of environmental mismatch on range estimation using waveguide invariant: theoretical analysis, simulations and experimental results', *IET Radar Sonar Navig.*, 2007, **1**, (4), pp. 274–280

[2] Ferri, G., Munafo, A., Tesei, A.*, et al.*: 'Cooperative robotic networks for underwater surveillance: an overview, simulations and experimental results', *IET Radar Sonar Navig.*, 2017, **11**, (12), pp. 1740–1761

[3] Fauziya, F., Lall, B., Agrawal, M.: 'Impact of vector sensor on underwater acoustic communications system, simulations and experimental results', *IET Radar Sonar Navig.*, 2018, **12**, (12), pp. 1500–1508

[4] Lamarre, E., Melville, W. K.: 'Sound-speed measurements near the ocean surface', *J. Acous. Soc. Am.*, 1994, **96**, (6), pp. 3605–3616

[5] Chen, X., Sun, C., Li, J.: 'Inversion of the sound speed profiles with an AUV carrying source using improved ensemble Kalman filter'. IEEE Int. Conf. Robotics Biomimetics, Qingdao, China, December 3-7, 2016

[6] Chen, J., Li, J., Wang, T.*, et al.*: 'Experimental demonstration of acoustic inversion using an AUV carrying source'. Int. Conf. Wireless Communications Signal Processing, Hangzhou, China, October 18-20, 2018

[7] Munk, W., Worcester, P., Wunsch, C.: '*Ocean acoustic tomography*' (Cambridge University Press, Cambridge, UK, 1995)

[8] Zhang, M., Xu, W., Xu, Y.: 'Acoustic tomography via matched field processing', *J. Acous. Soc. Am.*, 1991, **89**, (3), pp. 1119–1127

[9] Zhang, M., Xu, W., Xu, Y.: 'Inversion of the sound speed with radiated noise of an autonomous underwater vehicle in shallow water waveguides', *IEEE J. Ocean. Eng.*, 2016, **41**, (1), pp. 204–216

[10] Wang, T., Xu, W.: 'Sparsity-based approach for ocean acoustic tomography using learned dictionaries'. IEEE Oceans, Shanghai, China, April 10-13, 2016

[11] Bianco, M., Gerstoft, P.: 'Regularization of geophysical inversion using dictionary learning'. IEEE Int. Conf. onAcoustics, Speech, and Signal Processing (ICASSP), New Orleans LA, USA, March 5-9, 2017

[12] Bianco, M., Gerstoft, P.: 'Dictionary learning of sound speed profiles', *J. Acous. Soc. Am.*, 2017, **141**, (3), pp. 1749–1758

[13] Guo, X., Yang, K., Yang, Q.*, et al.*: 'Tracking-positioning of sound speed profiles and moving acoustic source in shallow water'. IEEE Techno-Ocean, Kobe, Japan, October 6-8, 2016

[14] Elisseeff, P., Schmidt, H., Johnson, M.*, et al.*: 'Acoustic tomography of a coastal front in Haro Strait, British Columbia', *J. Acous. Soc. Am.*, 1999, **106**, (1), pp. 169–184

[15] Aharon, M., Elad, M., Bruckstein, A.: 'K-SVD: an algorithm for designing overcomplete dictionaries for sparse representation', *IEEE Trans. Signal Process.*, 2006, **54**, (11), pp. 4311–4322

[16] Wang, X., Khazaie, S., Chen, X.: 'Linear approximation of underwater sound speed profile: precision analysis in direct and inverse problems', *Appl. Acous.*, 2018, **140**, pp. 63–73

[17] Carriere, O., Hermand, J. P., Le Gac, J. C.*, et al.*: 'Full-field tomography and Kalman tracking of the range-dependent sound speed field in a coastal water environment', *J. Marine Syst.*, 2009, **78**, pp. S382–S392

[18] Fang, R., Chen, T., Sanelli, P. C.: 'Towards robust deconvolution of low-dose perfusion CT: sparse perfusion deconvolution using online dictionary learning', *Med. Image Anal.*, 2013, **17**, (4), pp. 417–428

[19] Jensen, F. B., Kuperman, W. A., Porter, M. B.*, et al.*: '*Computational ocean acoustics*' (Springer, New York, NY, USA, 2011)

[20] Donoho, D. L.: 'For most large underdetermined systems of linear equations the minimal 1-norm solution is also the sparsest solution', *Commun. Pure Appl. Math.*, 2006, **59**, (6), pp. 797–829

[21] 'Underwater acoustics technical guides - speed of sound in sea-water', National Physical Laboratory, UK

[22] 'Determination of sound speed velocity from CTD data', Application Note no.6, Sea-Bird Electronics Inc., August 2004

[23] World Ocean Atlas 2018, Available at https://www.nodc.noaa.gov/OC5/woa18/

[24] 'World Ocean Atlas 2018 product documentation (prerelease)', Ocean Climate Laboratory, NCEI / NESDIS / NOAA

[25] Dahl, P. H., Zhang, R., Miller, J. H.*, et al.*: 'Overview of results from the asian seas international acoustics experiment in the east China sea', *IEEE J. Oceanic Eng.*, 2004, **29**, (4), pp. 920–928